ALT 12
Advanced Laser Technologies
2 – 6 September 2012, Thun, Switzerland

ALT 12
c/o Bern University of Applied Sciences
Engineering and Information Technology
Pestalozzistrasse 20, CH-3400 Burgdorf
info@alt12.org, www.alt12.org
0041 (0) 34 426 42 06

# NUMERICAL RECONSTRUCTION OF 3D IMAGE IN FOURIER DOMAIN CONFOCAL OPTICAL COHERENCE MICROSCOPY

Authors:

A. A. Grebenyuk, V. P. Ryabukho

DOI: 10.12684/alt.1.60

Corresponding author: A.A. Grebenyuk

e-mail: GrebenyukAA@yandex.ru

# Numerical Reconstruction of 3D Image in Fourier Domain Confocal Optical Coherence Microscopy

Anton A. Grebenyuk[1], Vladimir P. Ryabukho[1,2]

[1]Saratov State University, Astrakhanskaya str. 83, Saratov, 410012, Russia
[2]Institute of Precision Mechanics and Control, Russian Academy of Sciences, Rabochaya str. 24, Saratov, 410028, Russia

**Abstract**

Along with high longitudinal resolution of optical coherence tomography, confocal optical coherence microscopy (OCM) provides high transversal resolution due to relatively high numerical apertures. However, the presence of relatively high numerical apertures leads to limited depth of field, which reduces the speed of OCM and decreases the advantage of Fourier domain detection. In this paper we propose a numerical processing technique for three-dimensional image reconstruction in Fourier domain OCM. It takes into account not only the defocus of different parts of imaged volumetric sample, but also the effects of upper layers' refractive index on imaging the sample inner structure. Besides providing sharp coherence gated imaging, this technique also allows for determining both the geometrical thickness and refractive index of the sample layers.

**Introduction**

Low-coherence interferometry techniques allow three-dimensional imaging of semitransparent samples, based on longitudinal coherence gating, and are widely used in biomedicine [1,2]. In low-coherence interferometry the longitudinal coherence gating effect is caused by two factors: temporal and angular spectrum gates. Conventional optical coherence tomography (OCT) utilizes wide temporal spectrum and narrow angular spectrum of the optical field. Wide temporal spectrum leads to high longitudinal resolution, while narrow angular spectrum provides large depth of field. However, this narrow angular spectrum (due to low numerical apertures (NA)) leads also to low transversal resolution. To obtain high transversal resolution, higher numerical apertures are used, which provide wider angular spectrum of the optical field. However, wide angular spectrum results in small depth of field, which is in fact narrow longitudinal angular spectrum gate. This is the case of confocal optical coherence microscopy (OCM) [3]. So, one has to choose between imaging with either large depth of field and low transversal resolution or small depth of field and high transversal resolution [3].

To overcome this limitation in OCT, in Ref. [4] a numerical processing technique was proposed, based on synthetic aperture approach and inverse scattering analysis. It was shown to allow sharp sample imaging not only within the original depth of field, but also in defocused regions [4,5]. However, in Ref. [4,5] the effects of the refractive indices of upper sample layers on imaging its inner structure were not taken into account. Meanwhile, in a number of works [6-10] it has been shown for both confocal and full-field arrangements, that refractive index of the sample layers affects differently the location of temporal and angular spectrum gates. Mutual shift of these gates due to the mismatch of refractive index in sample and reference arms of an interferometer, leads to fading of the coherence signal. This effect limits applicability of the technique, described in Ref. [4,5], to imaging samples with uniform refractive index, equal to that of the immersion.

In Ref. [6,9,11,12] it has been shown, that this effect of coherence signal fading due to refractive index mismatch can be overcome in confocal and full-field arrangements by mechanical shifting of the temporal and angular spectrum gates. Along with sharp coherence gated imaging, it was shown to allow determination of both geometrical thickness and refractive index of the sample layers. However, the need for mechanical scanning makes these techniques time consuming and limit their applicability to *in vivo* imaging.

Recently, we developed a theoretical model of interference microscopy imaging to provide analysis of the imaging process of different types of samples in different types of interference microscopes [13-15]. Basing on this theory, we propose in the current paper a numerical processing technique, which is intended to overcome the problems of coherence gate fading in confocal OCM imaging and allow fast three-dimensional imaging of samples, which may consist of layers with different refractive indices, unequal to the refractive index of immersion.

**Image Formation in Confocal OCM**

Let's consider a confocal optical coherence microscope with signal acquisition in Fourier domain, which scans the sample transversal structure in transversal direction $(x_d, y_d)$. The coherence signal $\Gamma(\omega; x_d, y_d)$ obtained during this scan from an interface, located under $N$ sample layers with widths $\{\Delta z_j\}$ and refractive indices $\{n_j\}$ can be derived from the transmission functions, described in [14,15] to be

$$\Gamma(\omega; x_d, y_d) = \iint \tilde{\Gamma}(\omega; k_x, k_y) \times \exp[i(k_x x_d + k_y y_d)] dk_x dk_y, \quad (1)$$

where the spatio-temporal spectrum function $\tilde{\Gamma}(\omega; k_x, k_y)$ is determined by

$$\tilde{\Gamma}(\omega; k_x, k_y) = \Gamma_R(\omega) \prod_{j=1}^{N} t_{j-1,j}(\omega) t_{j,j-1}(\omega) \times \tilde{r}_S(\omega; k_x, k_y) \Xi(\omega; k_x, k_y), \quad (2)$$

where $\Gamma_R(\omega)$ is a coefficient, taking into account the properties of the reference arm and independent from the sample properties; $t_{j-1,j}(\omega)$ is a transmission coefficient from the $j-1$ th layer to the $j$ th; $\tilde{r}_S(\omega; k_x, k_y)$ is the spatial spectrum of the amplitude reflection coefficient distribution $r_S(\omega; x_S, y_S)$ of the interface of interest;

$$\Xi(\omega; k_x, k_y) = \iint dx_S dy_S \exp[i(k_x x_S + k_y y_S)] \times \iint A(\omega; x_3, y_3) \exp\left[ i k \sum_{j=0}^{N} \Delta z_j \sqrt{n_j^2 - \frac{x_3^2 + y_3^2}{f'^2}} \right] \times \exp[-i k (x_S x_3 + y_S y_3)/f'] dx_3 dy_3 \times \iint J_0(\omega; x_0, y_0) \exp\left[ i k \sum_{j=0}^{N} \Delta z_j \sqrt{n_j^2 - \frac{x_0^2 + y_0^2}{f'^2}} \right] \times \exp[-i k (x_S x_0 + y_S y_0)/f'] dx_0 dy_0, \quad (3)$$

where $A(\omega; x_3, y_3)$ is the aperture function of the microscope objectives; $J_0(\omega; x_0, y_0)$ is the illumination field complex amplitude distribution in the objective aperture plane; $k = \omega / c$ is the wavenumber; $c$ is the light speed in vacuum; $f$ and $f'$ are the front and back focal lengths of the objectives; $n_0 = n_{im}$ is the refractive index of immersion; $\Delta z_0 = z_S - |f|$; $z_S$ is the distance from the objective front principal plane to the sample surface.

It can be seen from Eq. (2) that the spatio-temporal spectrum of the acquired coherence signal is determined by the multiplication of the reflection coefficient spatial spectrum $\tilde{r}_S$ and the $\Xi$ function. In other words, the $\Xi$ function determines how accurately the coherence signal $\Gamma$ represents the structure of the sample interface of interest. The $\Xi$ function can be represented in the following way:

$$\Xi(\omega; k_x, k_y) = \Xi_t(\omega) \Xi_a(\omega; k_x, k_y), \quad (4)$$

where

$$\Xi_t(\omega) = \exp\left[ 2i k \sum_{j=0}^{N} n_j \Delta z_j \right], \quad (5a)$$

$$\Xi_a(\omega; k_x, k_y) = \Xi(\omega; k_x, k_y) / \Xi_t(\omega), \quad (5b)$$

which in parabolic approximation becomes

$$\Xi_a(\omega; k_x, k_y) = \iint dx_S dy_S \exp[i(k_x x_S + k_y y_S)] \times \iint A(\omega; x_3, y_3) \exp\left[ -i k \frac{x_3^2 + y_3^2}{2 f'^2} \sum_{j=0}^{N} \frac{\Delta z_j}{n_j} \right] \times \exp[-i k (x_S x_3 + y_S y_3)/f'] dx_3 dy_3 \times \iint J_0(\omega; x_0, y_0) \exp\left[ -i k \frac{x_0^2 + y_0^2}{2 f'^2} \sum_{j=0}^{N} \frac{\Delta z_j}{n_j} \right] \times \exp[-i k (x_S x_0 + y_S y_0)/f'] dx_0 dy_0 \quad (5c)$$

The functions $\Xi_t$ and $\Xi_a$ determine the longitudinal coherence gating effects in a confocal OCM caused by the temporal and angular spectra of the optical field. For convenience these coherence gating effects can be regarded to as temporal and angular spectrum gates.

In conventional Fourier domain OCT/OCM the sample structure is reconstructed by simple Fourier transform of the $\Gamma(\omega; x_d, y_d)$ function over the temporal spectrum $\omega$. In this Fourier transform for longitudinal position $\sum_{j=0}^{N} n_j \Delta z_j$, the phase modulation $\Xi_t$ over $\omega$ is eliminated and the image of the sample interface of interest is reconstructed. Meanwhile, this processing does not affect the $\Xi_a$ function, which produces modulation effect over the spatial frequencies of the spatio-temporal spectrum $\tilde{\Gamma}(\omega; k_x, k_y)$. It means that conventional Fourier domain OCT/OCM processing, affects only the position of the temporal spectrum gate, but does not affect the position of the angular spectrum gate, which results in degradation of the OCT/OCM signal, if the sample interface is out of the objective focus.

**Properties of the 3D Image and the Numerical Correction Procedure**

For correct imaging of the sample interface of interest, the correction of the spatio-temporal spectrum $\tilde{\Gamma}(\omega;k_x,k_y)$ for both modulations $\Xi_t$ and $\Xi_a$ is necessary. For this sake, we need first to analyze the properties of the $\Xi_a$ function, which affects the position of the angular spectrum gate. Fig.1 presents the dependence of the $\Xi_a$ function on the transverse spatial coordinates, calibrated in NAs ($k_x$ or $k_y$, as for circular apertures and illuminations, $\Xi_a$ has a circular symmetry) and on the amount of defocus $\Delta z_0$ for the case when the sample is simply a surface.

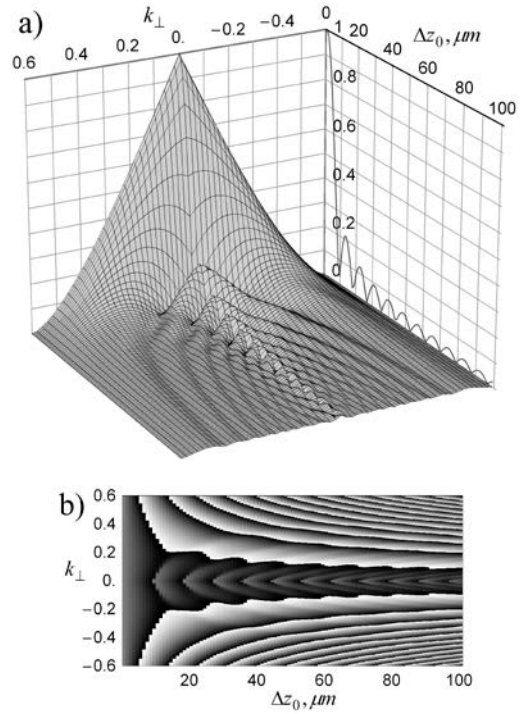


Fig.1 Analysis of the $\Xi_a$ function of an OCM with $NA = 0.3$, $\lambda = 800$ nm for different amount of defocus $\Delta z_0$: a) dependence of the $\Xi_a$ absolute value $|\Xi_a|$ on the transversal spatial coordinate $k_\perp = (k_x^2 + k_y^2)^{1/2}$ and the defocus $\Delta z_0$; b) dependence of the $\Xi_a$ phase $\arg(\Xi_a)$ on the transversal spatial coordinate $k_\perp = (k_x^2 + k_y^2)^{1/2}$ and the defocus $\Delta z_0$.

It can be seen from Fig.1b, that the phase modulation of $\Xi_a(\omega;k_x,k_y)$ over $(k_x,k_y)$ intensifies with increase of the amount of defocus. This means blurring of the images of the defocused sample parts. In can also be noticed from Fig.1a, that the amplitude of $\Xi_a(\omega;k_x,k_y)$ decreases with increase of the amount of defocus. It means that without appropriate correction, the images of the defocused sample parts are not only blurred, but also less intensive.

For correction of these effects it is necessary to divide the acquired spatio-temporal spectrum $\tilde{\Gamma}(\omega;k_x,k_y)$ by the $\Xi_a(\omega;k_x,k_y)$ function, computed for the desirable focusing depth inside the sample. However, care should be taken with the signal-to-noise ratio (SNR): as the absolute value of $\Xi_a(\omega;k_x,k_y)$ decreases with increase of $(k_x,k_y)$ and of the defocus, the direct division of $\tilde{\Gamma}(\omega;k_x,k_y)$ by $\Xi_a(\omega;k_x,k_y)$ would lead to decreased SNR for big $(k_x,k_y)$ or large defocus.

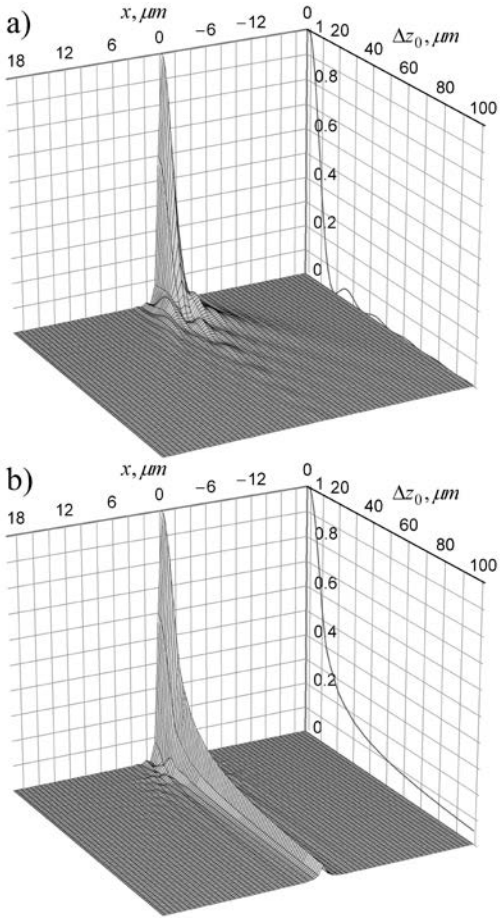


Fig.2 Analysis of the transversal PSF of an OCM with $NA = 0.3$, $\lambda = 800$ nm for different amount of defocus $\Delta z_0$: a) dependence of the initial PSF on a transversal coordinate $x$ or $y$ and the defocus $\Delta z_0$; b) dependence of the PSF after phase correction according to Eq. (6) on a transversal coordinate $x$ or $y$ and the defocus $\Delta z_0$.

To improve the OCM signal and avoid the problems with SNR, it is possible to perform only phase correction of $\tilde{\Gamma}(\omega;k_x,k_y)$, which means obtaining

$$\tilde{\Gamma}'(\omega;k_x,k_y) = \tilde{\Gamma}(\omega;k_x,k_y) \times \Xi_a^*(\omega;k_x,k_y)/\left|\Xi_a(\omega;k_x,k_y)\right|, \qquad (6)$$

As can be seen from Fig.2, this leads to sharpening and certain amplitude increase of the point-spread-

function (PSF) of the OCM system in defocused regions. Further multiplication of $\tilde{\Gamma}'(\omega;k_x,k_y)$ by $\Xi_t^*(\omega)$ and integration over $(\omega;k_x,k_y)$ yields a correctly reconstructed image, with both temporal and angular spectrum gates located at the same desired depth inside investigated sample.

It should be mentioned, that the form of the refractive index manifestation is different for the temporal and angular spectrum gates, which can be clearly seen from comparison of Eqs. (5a) and (5c). For every layer, a numerical variation of the temporal and angular spectrum gates positions and obtaining best possible images provides two equations for determination of the quantities $\Delta z_j$ and $n_j$. It means that this numerical processing technique provides the possibility of determining separately the values of $\{\Delta z_j\}$ and $\{n_j\}$, which has analogy with the full-field swept-source interference microscopy processing, described in Ref. [16,17].

### Effect of Numerical Correction on the Reconstructed 3D Images

For analysis of the effect of the numerical correction procedure on the reconstructed images in Fourier domain confocal OCM, we have performed numerical simulation of imaging a layered sample (Fig.3). The sample interface of interest is located under two layers with widths 20 μm and 25 μm and refractive indices 1.33 and 1.1 respectively; $NA = 0.3$, $n_{im} = 1$, the illumination field fills the whole objective aperture; central frequency of illumination $\omega_0 = 2.36 \times 10^{15}$ Hz (which corresponds to $\lambda_0 = 800$ nm), spectrum width $\Delta\omega = 3.53 \times 10^{14}$ Hz.

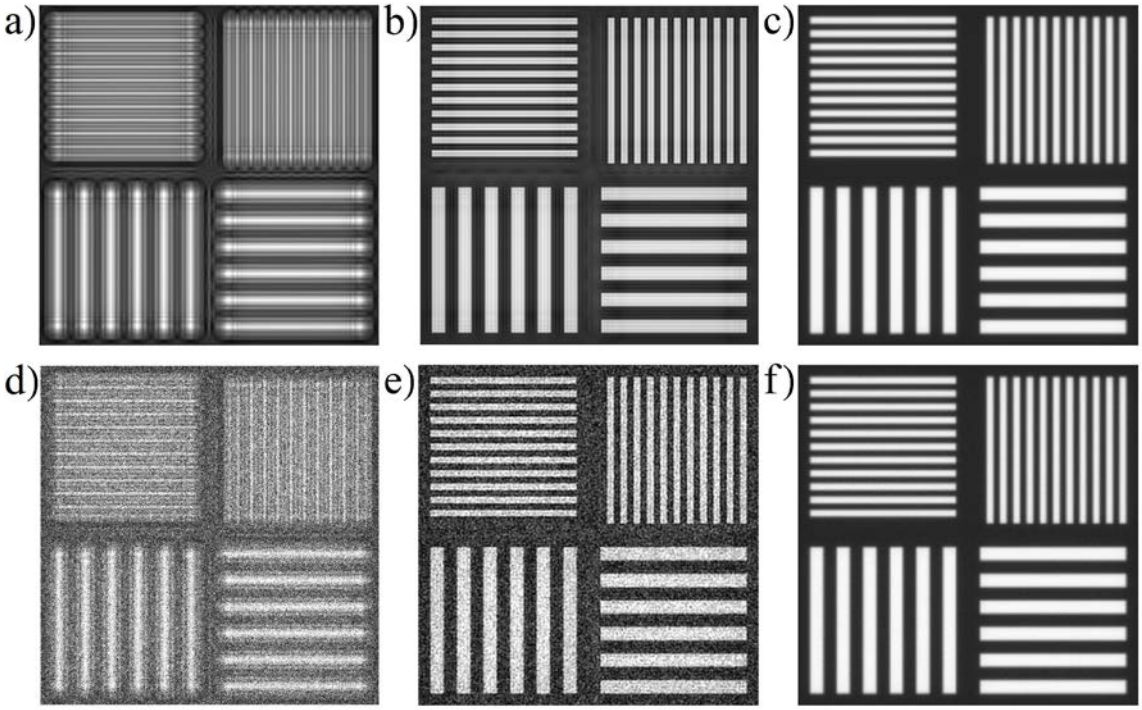


Fig.3 Numerical simulation of imaging a layered sample in Fourier domain confocal OCM. (a)-(c) without noise; (d)-(f) in presence of noise. (a), (b), (d), (e) the interface of interest is defocused (sample surface is in focus); (c),(f) the interface of interest is in focus. (a), (d) only temporal spectrum gate shifting is applied according to the conventional OCT/OCM principle; (b), (e) both numerical processing according to Eq. (6) and temporal spectrum gate shifting are applied. The field size for all images is 154×154 μm$^2$.

It can be seen from Fig.3a, that when only the temporal spectrum gate shifting is applied in accordance with the conventional OCT/OCM principle, the image of the defocused interface of interest is much blurred. The numerical correction procedure according to Eq. (6), allows for correct reconstruction of the image of this interface, without mechanical focusing on it (Fig.3b). It can also be seen from comparison of Fig.3d and Fig.3e, that the numerical correction procedure according to Eq. (6) leads not only to sharpening, but also to increase of SNR in the reconstructed image.

### Conclusions

In this paper we propose a numerical processing technique, which allows for correction of the longitudinal coherence gating effects and reconstruction of three-dimensional image in Fourier domain OCM. This technique takes into account the refractive index of the outer sample

layers on imaging its inner structure and provides the possibility of separate determination of the sample layers' thicknesses and refractive indices.

**Acknowledgements**

This work has been supported in part by RF Governmental contract 02.740.11.0879 and grant 1177.2012.2 "Support for the Leading Scientific Schools" from the President of the Russian Federation. We also gratefully acknowledge the support of SCOPES project, IZ74Z0_137423/1 (Switzerland, Russia and Uzbekistan) by Swiss National Science Foundation for participation in this conference ALT'2012.

**References**

[1] [Optical coherence tomography], W. Drexler and J. G. Fujimoto eds. (2008), Springer, Berlin, Heidelberg, New York.

[2] [Coherent-domain optical methods: biomedical diagnostics, environmental and material science], ed. V. V. Tuchin (2004), Kluwer Academic Publishers, Boston, 1 & 2.

[3] A. D. Aguirre and J. G. Fujimoto (2008), Optical coherence microscopy, in [Optical coherence tomography], W. Drexler and J. G. Fujimoto eds., Springer, Berlin, Heidelberg, New York, 505–542.

[4] T. S. Ralston, D. L. Marks, P. S. Carney and S. A. Boppart (2006), Inverse scattering for optical coherence tomography, Applied Optics 23(5), 1027-1037.

[5] T. S. Ralston, S. G. Adie, D. L. Marks, S. A. Boppart and P. S. Carney (2010), Cross-validation of interferometric synthetic aperture microscopy and optical coherence tomography, Optics Letters 35(10), 1683-1685.

[6] G. J. Tearney, M. E. Brezinski, J. F. Southern, B. E. Bouma, M. R. Hee, and J. G. Fujimoto (1995), Determination of the refractive index of highly scattering human tissue by optical coherence tomography, Optics Letters 20, 2258-2260.

[7] P. De Groot and X. C. de Lega (2004), Signal modeling for low-coherence height-scanning interference microscopy, Applied Optics 43(25), 4821-4830.

[8] V. Ryabukho, D. Lyakin and M. Lobachev (2005), Longitudinal pure spatial coherence of a light field with wide frequency and angular spectra, Optics Letters 30(3), 224-226.

[9] A. Dubois, G. Moneron and C. Boccara (2006), Thermal-light full-field optical coherence tomography in the 1.2 μm wavelength region, Optics Communications 266, 738-743.

[10] A. Safrani and I. Abdulhalim (2011), Spatial coherence effect on layer thickness determination in narrowband full-field optical coherence tomography, Applied Optics 50(18), 3021-3027.

[11] A. Dubois and A. C. Boccara (2008), Full-field optical coherence tomography, in [Optical coherence tomography], W. Drexler and J. G. Fujimoto eds., Springer, Berlin, Heidelberg, New York, 565-591.

[12] S. Labiau, G. David, S. Gigan. and A. C. Boccara (2009), Defocus test and defocus correction in full-field optical coherence tomography" Optics Letters 34, 1576-1578.

[13] A. A. Grebenyuk and V. P. Ryabukho (2012), Theoretical analysis of stratified media imaging in low-coherence interference microscopy, in Proc. SPIE 8337, 833707.

[14] A. A. Grebenyuk and V. P. Ryabukho (2012), Theoretical model of volumetric objects imaging in a microscope, Proc. SPIE 8430, 84301B.

[15] A. A. Grebenyuk and V. P. Ryabukho (2012), Coherence effects of thick objects imaging in interference microscopy, Proc. SPIE 8427, 84271M.

[16] A. A. Grebenyuk and V. P. Ryabukho (2012), Numerical correction of coherence gate in full-field swept-source interference microscopy, Optics Letters 37(13), 2529-2531.

[17] A. A. Grebenyuk and V. P. Ryabukho (2012), Numerical reconstruction of volumetric image in swept-source interference microscopy, Submitted in Proc. of "The 3rd Topical Meeting on Optical Sensing and Artificial Vision (OSAV'2012)", St. Petersburg, Russia, 14-17 May 2012.